Seasonal and interannual Salish Sea inflow origins using Lagrangian tracking

Becca Beutel[1], **Susan E. Allen**[1]

[1]Department of Earth, Ocean and Atmospheric Sciences, University of British Columbia, Vancouver, BC, Canada

Key Points:

- Quantitative Lagrangian tracking reveals the contributions of water masses to Salish Sea composition, and how these contributions vary
- Dominant inflow origins align with wind direction, north shelf and offshore in the summer, and south shelf and river plume in the winter
- Inflow in the winter varies significantly, while summer conditions remain relatively consistent

Corresponding author: Becca Beutel, `bbeutel@eoas.ubc.ca`

Abstract

The Salish Sea is a semi-enclosed sea between Vancouver Island and the coast of British Columbia and Washington State, invaluable from both an economic and ecologic perspective. Here we explore the contribution of Pacific water masses to the flow through Juan de Fuca Strait (JdF), the Salish Sea's primary connection to the Pacific Ocean. Quantitative Lagrangian particle tracking within Ariane, an offline Lagrangian tool capable of volume transport calculations, was applied to two numerical ocean models to track the paths and physical properties of water parcels before entering JdF (CIOPS) and within the Salish Sea (SalishSeaCast). During summer upwelling, flow from the north shelf and offshore dominate Pacific inflow, while during winter downwelling, flow from the south shelf and surface flow from the Columbia River plume are the dominant Pacific sources. A weaker and less consistent estuarine flow regime in the winter leads to less Pacific inflow overall and a smaller percentage of said inflow reaching the Salish Sea's inner basins than in the summer. Nevertheless, it was found that winter dynamics are a large driver of interannual variability. This analysis extends the knowledge on the dynamics of Pacific inflow to the Salish Sea and highlights the importance of winter inflow to interannual variability.

Plain Language Summary

The Salish Sea is a Northeast Pacific coastal sea, which supports large populations and biodiversity. The water that makes up the Sea is highly dependent on Pacific inflow through Juan de Fuca Strait (JdF). Knowing more about this water, and how it's composition changes between seasons and years, is important for assessing the Salish Sea's vulnerability to anthropogenic impacts. Water path was simulated to determine the origins of water entering the Salish Sea and reaching its inner basins. Summer inflow had remarkably consistent properties and trajectories. Winter inflow, however, was very variable; inflow was largely made up of two sources with distinct properties and erratic contributions to JdF inflow. Despite significantly more water flowing through JdF in the summer, variable winter inflow was found to be a critical component of the interannual differences in JdF conditions.

1 Introduction

1.1 Motivation and Overview

The Salish Sea is a semi-enclosed coastal sea between Vancouver Island and the coast of British Columbia and Washington State (figure 1a). This region is invaluable from both an economic and ecologic perspective: it supports large populations and economically important shipping routes, and is a critical ecosystem for the Pacific Coast (Gaydos & Pearson, 2011; Gaydos & Brown, 2011; Preikshot et al., 2013). Despite high productivity and stewardship and remediation projects, the Salish Sea has experienced large changes and fluctuations in certain marine populations (Preikshot et al., 2013), such as declines in Chinook salmon, which have been attributed to marine biogeochemical changes (Pearsall et al., 2021; Beamish et al., 2004). Monitoring and mitigating these changes is not simple, as the small size of the Salish Sea and its complex connection to the Pacific Ocean cause the conditions of this system, and other coastal regions, to be orders of magnitude more variable than in the open ocean - making accurate modelling a challenge (Giddings & MacCready, 2017; Fassbender et al., 2018).

Most water entering the Salish Sea does so through Juan de Fuca Strait (JdF) before reaching the productive and populated inner basins, the Strait of Georgia (SoG) and Puget Sound. Pacific inflow through JdF is the main contributor of many biologically important constituents (such as dissolved inorganic carbon (DIC) (Jarnikova et al., 2022) and nitrate (Sutton et al., 2013)) and pollutants (such as cadmium (Kuang et al., 2022)) to the Salish Sea, as well as a driver of variability therein. The composition of this inflow is a mixture of the water masses that are transported to the region via coastal currents, which change drastically between seasons due to shifts in dominant wind direction along the shelf and are at the whim of erratic atmospheric conditions in the region (Thomson et al., 2007; Thomson & Krassovski, 2010; Giddings & MacCready, 2017; Pawlowicz et al., 2019; Brasseale & MacCready, 2023) and has consequences for plankton diversity and biological productivity in the region (Belluz et al., 2021; Sutton et al., 2013).

Inflow make-up has been explored in papers such as Masson (2006), where the contributions of various sources of water to JdF and the SoG were quantified based upon their physical and chemical properties. The Pacific inflow is important year-round to SoG inflow, and the Columbia River inflow is significant to JdF surface water in the winter. However, all Pacific inflow through JdF was grouped together; thus, a gap in knowledge remains with respect to which Pacific water-masses make up this inflow and how their contributions vary annually and interannually.

1.2 Region Description

The Salish Sea is made up of five distinct regions (figure 1a): the SoG (the main deep region), Puget Sound (small interconnected basins), Haro Region (shallow channels with intense vertical mixing), Johnstone Strait (a narrow pass), and JdF (a straight channel connected to the Pacific). JdF inflow travels landward as intermediate (defined from a coastal perspective as 60-125 m) and deep water (>125 m), with lower density (fresher) outflow at the surface (Thomson et al., 2007; Ott & Garrett, 1998). Thickening of the estuarine outflow layer towards the northern shore occurs, since, unlike most estuaries, JdF is wide enough to be impacted by rotation (Labrecque et al., 1994). The strength of this flow changes seasonally (stronger in the summer) due to variable freshwater inputs from the region's rivers, most importantly the Fraser River, and variations in density of water on the shelf (Hickey et al., 2002).

Drastic changes also occur when wind conditions along the shelf shift from equatorward in the summer to poleward in the winter. Poleward winds drive onshore surface Ekman transport (Holbrook & Halpern, 1982), opposing the surface estuarine flow direction within JdF and, when they are strong enough, result in a pooling of the inflow along the southern shore and outflow along the northern shore, the transient flow regime (Thomson et al., 2007). This shift to the transient regime occurs about 10% of the time in the summer (April-September) and 45% of the time in the winter (October-March) (Thomson et al., 2007). The inflow during transient events is less well understood and may be made up of low salinity surface water from the northern Washington shelf, intermediate water that surfaces along the southern shore of JdF, or a combination of the two (Thomson et al., 2007; Giddings & MacCready, 2017). Importantly, the switch between regimes has large implications for how and what water is transported in and out of the region.

During estuarine flow, ∼70% of JdF inflow continues deeper into the Salish Sea while the rest is entrained into the upper layer (efflux transport) and advected out of JdF in the surface outflow (Pawlowicz et al., 2019; MacCready et al., 2021); however, it should be noted that water is also entrained from the surface layer into the inflowing intermediate layer in large quantities (reflux circulation, MacCready et al. (2021)). The water that does remain in the inflow is split (about 4:1) between the Haro Region to the north and Puget Sound to the South (Pawlowicz et al., 2019). Intense tidal mixing in the Haro Region leads to ∼85% of water returning to JdF in the surface layer instead of directly entering the SoG (Pawlowicz et al., 2019).

In addition to causing variable flow conditions within JdF, offshore winds have a large impact on the nature of the water entering the strait. Equatorward winds along the shelf in the summer initiate upwelling conditions, while poleward winds the rest of the year lead to downwelling (Foreman et al., 2011). The timing of the upwelling "season" varies from year to year; typically beginning at the start of April and ending at the start of October, but varies about these dates by almost a month (Hourston & Thomson, 2020). The difference in composition and flow behaviour of the upwelled water (namely higher in density compared to downwelled water) leads to the formation of an eddy over the shelf region (the Juan de Fuca Eddy, JdF-Eddy), and the flushing of deep SoG water in the summer (Foreman et al., 2008; Freeland & Denman, 1982; Pawlowicz et al., 2019).

Upwelling and downwelling conditions, and the shelf dynamics during these periods, bring about a varying sum of Pacific water masses (Thomson & Krassovski, 2010; Bograd et al., 2019) and local freshwater sources (Mackas et al., 1987) to the region. These water masses are transported to JdF through a complex network of currents (the California Undercurrent (CUC), the Davidson Current, the Shelf Break Current, the Columbia River Coastal Jet (CRCJ)), which vary in strength and extent throughout the year.

The CUC flows poleward in the subsurface along the continental slope nearly continuously, carrying a high density and high nutrient water (Hickey et al., 2002; Giddings & MacCready, 2017; Thomson & Krassovski, 2010); the Davidson current flows poleward at the surface over the shelf and offshore of the continental slope during periods of downwelling, carrying southern shelf water (Giddings & MacCready, 2017; Thomson & Krassovski, 2010); the Shelf Break Current is a wind driven current that flows equatorward over the continental slope in the summer, carrying northern slope water (Thomson et al., 1989; Ikeda & Emery, 1984; Hickey, 1998; Thomson & Krassovski, 2010) and acts as the shelf extension of the California Current (CC) (Giddings & MacCready, 2017; Chenillat et al., 2012); the CRCJ is made up of warm and fresh water from the Columbia River (200 km south of the mouth of JdF), flowing quickly poleward during southerly winds and downwelling conditions, with little mixing as it travels up the coast (Thomson et al., 2007; Hickey et al., 2009; Giddings & MacCready, 2017). Understanding the behaviour of these currents, and importantly the distinctions between the water they carry, is key to interpreting the interannual and seasonal variability in JdF inflow composition.

1.3 Lagrangian Tracking

This study applies Lagrangian tracking to the analysis of transport of water into the Salish Sea and to its inner basins. Previous analysis has been done from an Eulerian perspective (e.g., Khangaonkar et al., 2017; Thomson et al., 2007), providing an important overview of mean currents. Tracer based analysis (e.g., Pawlowicz, 2001) has also been applied, but separating tracer diffusion and advection from overall transport can be extremely difficult (Stevens et al., 2021), particularly in systems where sources have overlapping tracer characteristics.

Lagrangian ocean analysis tracks free moving entities, real (e.g., Paris et al., 2013; Pawlowicz et al., 2019) or virtual (e.g., Stevens et al., 2021; Brasseale et al., 2019), to estimate ocean pathways by applying the Lagrangian lens of fluid dynamics (Bennett, 2006). In a virtual sense, this method tracks an ensemble of simulated water parcels to see their path and how their compositions change along this path based on the time varying velocity fields of an ocean model (Van Sebille et al., 2018); often leading to complex and unpredictable paths (LaCasce, 2008). Virtual tracking also allows for backwards simulations of parcel movement, leading to enhanced water mass source analysis, based on the path water parcels take to get to a region without the bias of seeding particles from assumed sources (e.g., Sahu et al., 2022). Despite the complexities of Lagrangian analysis, the incorporation of time varying velocity and the ability to conduct backwards integrations allows for source water contribution analysis to a level of accuracy unmatched by other analysis techniques of similar computational costs (Davis, 1994; Van Sebille et al., 2018).

In this paper the trajectories and physical properties of water parcels in the Sea and on the shelf were tracked forwards and backwards in time, respectively, based on the circulation from two numerical ocean models in order to determine the composition of water entering the Salish Sea through JdF. We quantify the contribution of different sources of JdF inflow and investigate the pathways within the Salish Sea to assess which Pacific sources are important to JdF and the inner basins, and how the significance of these sources differ between seasons and years.

2 Methods

2.1 Models

The regional numerical ocean model outputs analysed in this study are from SalishSeaCast, a 3D physical-biological-chemical ocean model, and the Canadian Ice Ocean Prediction System (CIOPS) for the West Coast, an atmosphere-ocean-ice forecasting system. Both models are applications of the Nucleus for European Modelling of the Ocean (NEMO) version 3.6 model architecture (Madec & the NEMO team, 2016) and, while they differ in resolution and spatial extent, overlap completely in the Salish Sea.

2.1.1 SalishSeaCast

A five year subset (2016-2020) of hourly 3D SalishSeaCast version 201905 output was used. SalishSeaCast is described in detail in Soontiens et al. (2016) and Soontiens & Allen (2017), and updates to the model since then are summarized in Olson et al. (2020) and Jarnikova et al. (2022).

Temperature and salinity boundary conditions at the mouth of JdF are based upon fields from LiveOcean (MacCready et al., 2021) with tidal heights and currents at the boundary forced, and then tuned (Soontiens et al., 2016), using eight tidal components (K1, O1, P1, Q1, M2, S2, N2, and K2) initially from Webtide (Foreman et al., 2000). Model bathymetry is based upon measurements from the Canadian Hydrographic Service (Olson et al., 2020) with gaps filled using a 3 arc-second digital elevation model (Sutherland, 2013) or the Cascadia physiography dataset (Haugerud, 1999), smoothed for model stability (Soontiens et al., 2016). Fraser river flow is based upon Environment and Climate Change Canada's (ECCC) gauge in Hope, BC, while smaller rivers are forced from climatology (Morrison et al., 2012). Atmospheric forcings are from 2.5 km output of ECCC's High Resolution Deterministic Prediction System (HRDPS) (Milbrandt et al., 2016).

The model has a horizontal resolution of about 500 m and a vertical resolution ranging between 1 m at the surface and 27 m at a depth of 430 m. The height of every grid-cell is stretched and compressed according to the model's sea surface height (ssh) in order to simulate the change in sea-level from tides (Olson et al., 2020; Levier et al., 2007).

Evaluations of SalishSeaCast output have yielded favorable results; the model captures temporal and spatial variability in physical tracer concentrations and resolves known dynamics. When compared to observations the Willmott skill score (WSS) in model physics is 0.96-0.98 for potential temperature and 0.83-0.98 for salinity (Olson et al., 2020). The model has been found to be slightly colder (bias of -0.04° C and root mean squared error (RMSE) of 0.63) and saltier (0.02 $\mathrm{g\,kg^{-1}}$ bias and 0.82 RMSE) compared to hydrographic surveys over the thalweg (average measurement depth of 72 m), and warmer (0.13 ° C bias and 1.12 RMSE) and fresher (-0.74 $\mathrm{g\,kg^{-1}}$ bias and 2.28 RMSE) near the coast (average measurement depth of 10 m) (Olson et al., 2020). Horizontal Lagrangian diffusivity from the model matches well with that from drifter observations (Stevens et al., 2021) and is more than 10x larger than the imposed sub-grid scale diffusivity.

2.1.2 CIOPS

An 18 month subset (October 2016 - March 2018) of the CIOPS model output, fields of 3D daily average velocity and 2D hourly barotropic velocity, was used. A previous iteration of the model is described in detail in Lu et al. (2017) and the updates that reflect the model applied in this study are explained in Holdsworth et al. (2021) and Sahu et al. (2022).

Boundary conditions for the daily mean velocities, and non-tidal ssh at the model boundaries are from PSY4 (Lellouche et al., 2013) while those for tidal depth-average velocity and ssh are based upon eight tidal components (K1, O1, P1, Q1, M2, S2, N2, and K2) from Webtide (Foreman et al., 2000). Atmospheric forcings in the model are based on Climate Forecast System Version 2 (Saha et al., 2014) and rivers forcings are based upon climatology (Morrison et al., 2012).

CIOPS has a resolution of 1/36° in the horizontal and a vertical resolution of ranging between about 1 m at the surface and 200 m at a depth of just under 6 km, as in SalishSeaCast, partial cells at the bottom are used to reflect the complex bathymetry of the region (Holdsworth et al., 2021). Cells are stretched and compressed in the hourly output to represent tidal changes in ssh (Levier et al., 2007).

Tides are a significant driver of estuarine circulation in JdF (MacCready et al., 2021; Becherer et al., 2016), but are not captured in the daily 3D CIOPS output. However, hourly barotropic velocities are archived. Thus, CIOPS model output was converted to 3D hourly output based on the relationship that velocity is the sum of the barotropic and baroclinic velocities, with the assumption that the diel variation in the baroclinic component of the tides was minimal (Beutel, 2023a).

Comparisons to moving vessel profiler data collected in 2013 around Juan de Fuca Canyon (JdF-Canyon) suggest that the CIOPS model has a slight warm bias throughout the water column, particularly at the surface, and a slight fresh bias at the surface and saline bias at depth (Sahu et al., 2022). This evaluation yielded strong WSSs of of 0.94 and 0.93, RMSEs of 1.09° C and 0.38 PSU, and bias values of 0.19° C and 0.33 PSU for temperature and salinity, respectively (Sahu et al., 2022). Comparisons to a mooring west of the entrance to JdF (48.53°N, 126.2°W, ∼500 m depth) revealed a close match between model and observed velocities in the top 200 m, with a WSS of 0.71 and RMSE of 0.08 $\mathrm{m\,s^{-1}}$ (Sahu, 2019). The CUC is shifted offshore in the model however, leading to slower than observed velocities against the slope at depths >=200 m (Sahu, 2019).

2.2 Particle Tracking

Lagrangian simulations were done using Ariane, an offline Lagrangian tool capable of 3D parcel trajectory and volume transport calculations in its quantitative mode (e.g., Schmidt et al., 2021; Hailegeorgis et al., 2021; Vecchioni et al., 2023). Ariane integrates water parcel paths either forward or backwards in time (forwards for the study of pathways, backwards for source water analysis) based on velocity fields from an ocean model by calculating 3D streamlines (assuming local non-divergence) within the cell in which a parcel is located at each time-step (Blanke & Raynaud, 1997). No sub-grid scale mixing is included within Ariane; however, temperature and salinity are interpolated from the underlying model, implicitly incorporating the sub-grid scale mixing and diffusion of tracers from it (Sahu et al., 2022; Schmidt et al., 2021). While some random flow is lost by ignoring sub-grid scale mixing, major flow paths are followed and backwards tracking becomes possible (Van Sebille et al., 2018).

In the quantitative mode water parcels are continuously seeded along an "initialisation" section, where parcel distribution is based on the transport through each cell, and tracked between there and simulation boundaries defined by the user on the model-grid (ex. figures 1b and c). Each water parcel is assigned a flux, so that the total flux through the boundary is represented (Blanke & Raynaud, 1997). Due to the plethora of parcels tracked, information on them is only recorded once they have passed one of said boundaries.

Water parcel seeding in both simulations occurred at an initialisation boundary (figure 1b and c) inland of the mouth of JdF east of Port Renfrew (figure 1a), hereafter referred to as Port Renfrew Transect (PRT), as flows at the mouth may not reflect the water that actually enters the Salish Sea. In SalishSeaCast forward quantitative integrations of particle trajectories were run to examine the flux and physical properties of water parcels originating at PRT and reaching the inner basins (figure 1b). Particles were seeded every hour for a year and tracked for an additional thirty days after that year was complete, with five simulations of one year each (2016-2020).

In CIOPS, particles were tracked in reverse from PRT (backwards integration) to determine the shelf sources of particles that reach PRT and contribute to the inflow tracked in the SalishSeaCast runs (figure 1c). The northern section terminates at the 1000 m isobath, while the southern section extends further offshore (figure 1). This difference in where the offshore section intersects the north and south is due to the definitions of currents in the region (Giddings & MacCready, 2017): in the north the shelf break current is the shelf extension of the CC, the delineation between it and its offshore manifestation occurs at the continental slope; in the south the Davidson current flows at the surface over the shelf and offshore and the CUC flows along the continental slope, so the division with offshore water occurs further from the coast. Eighteen months of particle seeding every hour (March 2018-October 2016), with thirty extra days of tracking, was conducted. While these models are used together to assess the Pacific sources of water into the Salish Sea and its inner basins, it is important to note that there is no direct passage of particles between the two models. In section 3.1, we discuss the consistency between the models.

Average transport across simulation boundaries is calculated by summing the transport of each parcel that crosses the boundary in a chosen time-period, divided by the number of time-steps with particle seeding in said time-period. For example, if one was interested in fluxes across a section in a single month, one would sum the transport of all parcels crossing a given transect in that month (based upon the "final section" and "final time" of a parcel in Ariane) and divide by the number of time steps in the entire month (ex. 24 hours x number of days in the month in the case of this analysis).

2.3 Water classification

Sources and destinations of water parcels are based upon their position, and in some cases salinity, at the end of backwards and forwards runs, respectively. Water parcels that do not reach any of the set boundaries during the simulation are considered "lost" while parcels that pass back over PRT are referred to as "loop(ed)" parcels.

Looped water parcels that pass back over PRT within one day of being seeded are removed from analysis as these parcels simply passed back and forth over PRT due to tidal pumping and are not relevant for source water analysis. Looped water parcels that last longer than one day in the simulation are considered to be strait outflow in CIOPS analysis, and entrained (efflux circulation) or wind-driven looped water parcels in SalishSeaCast analysis.

Divisions between source waters (table 1) along the southern boundary in CIOPS (figure 1c) are based upon seasonal TS diagrams of water parcels at this crossing (figure S4) and previous studies on the physical properties of the CUC (Huyer et al., 1998; Masson, 2006; Sahu et al., 2022). The disconnect between the two models means that the water parcels in SalishSeaCast cannot be directly attributed to specific shelf sources. In SalishSeaCast the division of water parcels at PRT is based upon the location of major flow cores in the model, and definitions of layer depth in JdF inflow (Thomson et al., 2007; Thomson, 1981). CIOPS results at PRT increase our understanding of the contributions of shelf sources to these inflows, but importantly shelf flow is not the only contributor to JdF inflow (and by extension the sources analysed in SalishSeaCast simulations): return flow, reflux circulation, and local rivers also contribute. Details on the delineation of source waters and the sensitivity of the results to this choice are expanded upon in supplement S1.

Analysis of CIOPS inflow location and properties was split into winter 2016/17 (October 2016-May 2017), summer 2017 (June - September 2017), and winter 2017/18 (October 2017-March 2018) based on the initiation and ending of upwelling. To put these 18 months in context, using the five years of SalishSeaCast analysis, summer 2017 had

Table 1: Source water definitions for water parcels in the CIOPS (figure 1c) and SalishSeaCast (figure 1b) simulations.

CIOPS Source	Shelf Boundary Position and Additional Requirements
North Shelf	North
Offshore	Offshore
South Shelf	South, $33.9\,\text{g kg}^{-1} >$ salinity $\geq 32\,\text{g kg}^{-1}$
South Deep	South, salinity $\geq 33.9\,\text{g kg}^{-1}$
Columbia River	South, salinity $< 32\ \text{g kg}^{-1}$
Strait Outflow	PRT, transit time > 24 hours
SalishSeaCast Source	**PRT Position and Additional Requirements**
Surface	<150 m deep, salinity $< 32\ \text{g kg}^{-1}$
Intermediate	<150 m deep, salinity $\geq 32\,\text{g kg}^{-1}$
Deep	≥ 150 m deep

slightly higher total inflows but was otherwise typical, winter 2016/17 had low flow and mean salinity at the beginning of the season and high mean temperature throughout, and winter 2017/18 had typical temperatures but the largest seasonal variability and range in both flow magnitude and salinity.

3 Results

3.1 Model Comparison

The similitude of SalishSeaCast and CIOPS within JdF was assessed to ensure that the two models could be used in unison to study JdF inflow. The temperature and salinity observations at Ocean Network Canada's JF2C Mooring near PRT (latitude = 48.360° N, longitude = 124.213° W, depth = 175 m) were compared to temperature and salinity model output. Both models showed a fresh bias of $0.2\ \text{g kg}^{-1}$, with WSSs and RMSEs of 0.79 and $0.21\ \text{g kg}^{-1}$, and 0.83 and $0.15\ \text{g kg}^{-1}$ in SalishSeaCast and CIOPS, respectively. SalishSeaCast revealed a small cool bias of 0.09° C while CIOPS has a more significant warm bias of 0.52° C, with WSSs and RMSEs of 0.91 and 0.36° C, and 0.89 and 0.43° C in SalishSeaCast and CIOPS, respectively.

Based upon the seasonally varying temperature of Columbia River outflow (Beutel, 2023a), it was found that temperature would not be a useful measure for differentiating between southern water masses - thus, the weaker match between this parameter in the two models is not a concern for water mass differentiation.

Inflow in both models at PRT was similar, based on horizontal velocities across PRT in the models, with CIOPS less by 5-10% of the flux in SalishSeaCast. Due to the resolution difference between the two models however, the shape of this inflow differs slightly. Notably, during periods of transient flow, the brackish surface inflow is spread relatively evenly over the entire width of JdF in CIOPS, instead of focused on the southern side of the channel as expected from observations (Thomson et al., 2007) and seen in SalishSeaCast results (figure 5). As surface inflow through JdF is defined in this study by its salinity, this shape difference should not influence the surface inflow discussed in the following sections.

3.2 Quantitative Lagrangian Tracking

In both simulations and at all times the majority of water at PRT was found to be tidally pumped (water that passes back over PRT in less than two tidal cycles), over 76% (79%) of total flow in the summer (winter) in CIOPS simulations, and around 67% (72%) in the summer (winter) in SalishSeaCast simulations. The results outlined in the following sections do not include these tidally pumped parcels.

3.2.1 Into JdF, Summer

The inflow in the summer reaches JdF from all directions (figure 2). Water parcels from the North (28%), Offshore (27%), and strait outflow (26%) account for most of the flow reaching PRT, however water from the south sources are not negligible (together 19%) (table 2). A strong core of flow along the northern section can be observed, while water parcels are diffuse across the offshore section (figure 2). Looking at the flow across the offshore section in the summer over a significantly smaller flux range (figure S2) shows that a higher concentration of offshore water originates towards the northern end of the section down to 300 m.

Most of this inflow passes through the region of the JdF-Eddy before flowing into JdF, leading to a mixing of the water masses and a convergence of properties before reach-

Table 2: Percentage of flow from CIOPS sources to PRT, at PRT in SalishSeaCast, and from PRT to the inner basins in SalishSeaCast in summer 2017, and winters 2016/17 and 2017/18, as well as five year averages of SalishSeaCast summer and winter source paths. Percentages are based upon the contributions of each source, defined in table 1, to non-tidal transport.

	Summer 2017	Winter 2016/17	Winter 2017/18	Summer Average	Winter Average
Shelf to PRT					
North Shelf	28%	0%	2%		
Offshore	27%	2%	4%		
South Shelf	10%	32%	31%		
South Deep	8%	2%	7%		
Columbia River	1%	11%	8%		
Strait Outflow	26%	53%	48%		
Source at the PRT					
Surface	1%	16%	16%	2%	14%
Intermediate	73%	56%	57%	72%	57%
Deep	25%	28%	27%	26%	29%
PRT to inner basins					
Surface					
Looped	97%	87%	83%	96%	86%
to Haro	2%	9%	9%	3%	8%
to Puget Sound	1%	4%	6%	1%	5%
Intermediate					
Looped	41%	54%	56%	44%	53%
to Haro	48%	36%	32%	46%	35%
to Puget Sound	10%	10%	10%	10%	10%
Deep					
Looped	56%	69%	67%	60%	66%
to Haro	37%	25%	24%	33%	25%
to Puget Sound	6%	6%	7%	6%	7%

ing PRT (Beutel, 2023a). Strait outflow properties however change very little between leaving PRT and becoming part of PRT inflow (ibid).

Strait outflow parcels, having the smallest distance to travel, are the fastest to reach PRT with most water parcels arriving shortly after 24 hours and decreasing in numbers after 8 days (figure 3b). Of the outer boundary water parcels, south deep water parcels are the first to reach PRT (14 days) but have the slowest peak age (56 days). North shelf parcels begin to reach PRT shortly after south deep water parcels (16 days), have one major peak at 37 days and show little variation in timing. South shelf parcels also begin to arrive after 16 days with two peaks in inflow age, a first quick but smaller peak (27 days) and a second, larger, peak (54 days). Offshore parcels are the last to arrive (19 days) and have a wider spread in timing than the other water masses, with over four times more particles reaching PRT after the peak (42 days) than before.

3.2.2 Into JdF, Winter

Despite there being weaker surface outflow in the winter, returning strait outflow is even more dominant a source, at 53% and 48% of the total inflow in winters 2016/17 and 2017/18 (table 2), respectively; a core of strait outflow is visible leaving PRT at the surface on the southern side as well as a weaker signal below 100 m on the northern side (figure 2). Of the outer boundary (Pacific) sources, southern shelf water is the most significant source in both winters (on the southern continental slope, figure 2), 32% of the inflow in winter 2016/17 and 31% in winter 2017/8. It should be noted however, that while the southern source is similarly important overall in both winters, its percentage contribution fluctuates on daily timescales, responsible for between nearly none and all of the Pacific inflow (figure 4a), with no clear temporal trend over the season.

The Columbia River inflow becomes important in the winter (adjacent to the southern shore, figure 2), at 11% and 8% of the total inflow in winters 2016/17 and 2017/18, respectively. Combined, the south and Columbia River make up 80% or more of the Pacific inflow throughout the winter but are poorly correlated on daily timescales (figure 4a).

The Columbia River water reaches PRT faster than the southern shelf water (figures 3a and c); particles begin to arrive only three days after seeding and decrease quickly after peaking at only five days. The fastest south shelf water parcels arrive at the peak time for Columbia River inflow (four days after seeding) with most parcels arriving after its peak arrival age of 17±1 days after seeding (depending on the winter). South deep water parcels arrive (10 days) and peak (27±3 days) faster than they did in the summer. Like in the summer, the strait outflow water parcels begin to arrive immediately, peak quickly, and decrease shortly thereafter (11 days) (figure 3).

3.2.3 Within the Salish Sea

Significant amounts of JdF inflow is advected back out to sea before reaching either of the inner basins, averaging 49% of the total inflow during the summers of 2016-2020, and 61% in the winters. Overall flow magnitude changes seasonally; flows into the Haro Region in particular are high in the summer and low in the winter (figure S1a). Sample cross sections of inflow in JdF in the winter (month average of January 2018, figure 5b) and summer (month average of May 2018, figure 5a) highlight the difference between the estuarine and transient flow states. In the summer, little to no positive velocities are seen outside of the main inflow region (figure 5c). Winter inflows have significantly lower velocities and, unlike the summer inflows, the shape of the inflow is not consistent, with scattering of positive velocities throughout the cross-section and significant variability in the flow structure outside of the main core (figure 5d).

Significantly more variability in the inflow properties was found in the winter months (figure 6). In the summer, the inflow salinity and temperature for all five years of the simulation is grouped into a few bins with little variability therein. In the winter the salinity and temperature bins responsible for most of the water parcels changes between years, and the inflow is made up of diverse concentrations.

As shelf trajectory information is not available in the SalishSeaCast simulations, water masses are more generally grouped into deep, intermediate, and surface water based upon their depth and salinity (table 1). Surface water, for example, is not solely from the Columbia River plume in this case as it is a mixture of this plume, JdF outflow, and smaller rivers along the coast.

Surface water is most susceptible to being advected out of JdF (table 2); little (on average 4% of the surface inflow at PRT) surface inflow reaches the inner basins in the summer. In the winter, while stronger than the summer, at 13% is still more susceptible to being entrained than the other sources.

Unlike surface inflow, more intermediate and deep water penetrates the inner basins in the summer than in the winter. In summer on average 39% of the deep and 56% of the intermediate water made it to the Haro Region or Puget Sound. In the winter this penetration percentage decreases to 32% of the deep and 45% of the intermediate source.

Intermediate water is consistently the largest source of flow into both the inner basins (figures S1b and c). Deep flow into both basins does not follow a strong seasonal cycle while surface inflow to both varies significantly between the summer and winter (figures S1b and c).

Mixing of these water masses before reaching the inner basins leads to a convergence of their densities and a similar inflow shape into each channel; however, not all water masses behave the same. The contribution of the fresher surface water to channel inflow is comparable between Haro Strait and Admiralty Inlet in the winter (figures S1b and c) despite Haro Strait total inflows being much higher (figure S1a), and Puget Sound inflow is consistently lower in density than the water entering the Haro Region.

4 Discussion

Lagrangian trajectory and property results from offshore and Salish Sea analysis highlight the complex flows of the region and reveal important distinctions between summer and winter conditions. Summer inflow properties and magnitude into JdF and the inner basins show minimal interannual variability and the inflow is largely made up of north and offshore water traveling at intermediate depths (figure 7a) and well correlated in time. Winter inflow properties and magnitude are variable between years and within a single season with the majority of flow made up of two poorly correlated water masses, the shelf water from the south traveling at intermediate depths and Columbia River outflow traveling at the surface (figure 7b).

4.1 Water Parcel Dynamics

4.1.1 To PRT

The marked differences between the seasons appear to connect well to the wind over that period (figure 4b), with consistent equatorward winds in the summer until the fall transition (around September in 2017) when all Pacific water masses play a significant role (figure 4a), and erratic poleward winds in the winter months contributing to quick switches in the water masses contributing to JdF flow. The flow of major rivers (figure 4c) however, seems to have a smaller impact; with high Columbia River flows in the spring of 2017 not equating to high Columbia River contributions to JdF for example. While variation in Fraser River flow contributes to the strength of estuarine exchange it does not appear to impact which water masses make up the inflow.

During upwelling, wind driven equatorward surface flow predominantly carries northern shelf water and offshore water to the region. The large contribution of offshore water to Pacific inflow at PRT was unexpected, as the inflow to an estuarine system such as JdF is expected to originate from the shelf or continental slope (Brasseale & MacCready, 2021), and previous estimates of sources of Salish Sea inflow have assumed sub-surface JdF inflow to originate from the shelf (e.g., Masson, 2006). While offshore parcels originate in small amounts over the whole section, the higher concentration towards the northern end at depths shallower than 300 m suggests that this water may be an offshore extension of the shelf-break current - in line with our understanding of the connection between the shelf-break current and the CC in the summer (Giddings & MacCready, 2017; Chenillat et al., 2012)). The timing of offshore and northern water are highly correlated ($R = 0.73$, figure 4) and contribute similar magnitudes to JdF inflow (36% and 38% of Pacific inflow respectively, figure 7), meaning that similar shelf conditions carry north shelf and offshore water parcels to PRT.

While the timing of flow from the offshore and north boundaries are well correlated (figure 4), the average (and range in) simulation time of water parcels from the north boundary is less than from the offshore boundary (figure 3b). Offshore water parcels experience a large range of conditions; many of the offshore parcels begin below depths of 200 m (figure S2) and are upwelled within the bounds of analysis, and the offshore boundary extends from north to south of the mouth of JdF (figure 1c) with some particles originating from the southern portion of the boundary, contrary to the dominant wind direction. More water parcels originate from the northern end of the boundary (figure S2) but do not behave exactly like northern water parcels; most water parcels cross parts of the offshore cross section perpendicular to the northern boundary (figure 1c).

Shelf and offshore contributions to deep PRT inflow is relatively consistent, from 15 milli-Sverdrups ($\text{mSv} = 10^3\ \text{m}^3\text{s}^{-1}$) in summer 2017 down to 8 and 10 mSv in the analysed winters (figure 7). Winter versus summer initial arrival of south deep water parcels to PRT also does not differ as significantly, 15 days in the summer and 12 and 10 days in winter 2016/17 and 2017/18 respectively (figure 3). This relative similarity between seasons may be explained by the consistent flow of deep water reaching PRT via the JdF-Canyon (figure S3). However, while this consistency is of interest, deep water transport into JdF is significantly lower than expected, potentially due to the low resolution of the JdF-Canyon or the location of the CUC in CIOPS, as discussed further in section 4.2.1.

In the winter, the wind-driven poleward Davidson Current (Thomson & Krassovski, 2010) drives southern shelf water to dominate Pacific sources into JdF (figure 7b). The poleward wind also contributes to a much faster transit time for the southern parcels (figure 3) in the winter (peak at 16-18 days) versus the summer (smaller peak at 24 days and larger at 55). The two age peaks in the summer reflect a difference in timing between south water parcels that flow through the JdF-Eddy (slower) and those that pass along the JdF-Canyon or closer to the shore (figure S3b); in the winter all southern water parcels travel along either the JdF-Canyon or closer to shore (figures S3c and d).

Winter conditions also introduce the presence of the Columbia River plume into JdF inflow. The daily Columbia river inflow and southern shelf inflow are poorly correlated (figure 4), combined accounting for over 80% of the Pacific flow reaching PRT at any given time. This weak relationship is likely related to the strength of poleward winds - while both sources may travel poleward under similar conditions, south shelf water can do so during the relaxation of upwelling conditions (Sahu et al., 2022) while the Columbia River plume only travels northward during downwelling conditions paired with strong poleward wind events (Thomson et al., 2007; Hickey et al., 2009; Giddings & MacCready, 2017). The Columbia River plume has also been found to inhibit shoreward surface transport (Giddings et al., 2014), potentially blocking the southern shelf inflow to PRT when poleward winds are particularly strong.

The movement of the Columbia River water parcels along the coast is faster than any of the other water masses, taking three days from the southern boundary due to the characteristic strong winds that carry it northward (figure 3a and c). The Columbia River plume maintains the lowest salinity and highest temperature of the water masses, with little change in its properties and therefore little mixing over its path, consistent with previous studies of the plume water as it travels north (Giddings & MacCready, 2017).

The seasonal and interannual changes in water masses entering the Salish Sea culminates in significant differences between the salinity and temperature of water carried into the region between seasons and between years. The majority of Pacific water reaching PRT in the summer has properties (high salinity and low temperature) characteristic of upwelled water (figure 6). The small range in summer properties suggests a reasonable consistency in the water masses reaching PRT during upwelling in the five years of SalishSeaCast analysis.

The winter water parcel properties exhibit more variability and diversity. Inflow temperatures are relatively warmer and salinities decrease due to the end of upwelling conditions. The breadth of properties reaching PRT (figure 6) align with the distinct difference between source waters in the winter, as well as how the properties of those sources change throughout the winter and between years despite their path remaining the same (eg. the seasonal temperature cycle of the Columbia River). The variability between years further demonstrates how the contribution and the properties of these different sources are not consistent.

4.1.2 Beyond PRT

Lagrangian tracking gives lower PRT inflow to the inner basins (figure 7) than that based upon salinity and temperature observations, where 70% of JdF inflow reached the Haro Region or Puget Sound in both summer and winter (Pawlowicz, 2001; Pawlowicz et al., 2019). Intermediate water, largely north and offshore water in the summer and south shelf water in the winter, contributes the most to inner basins inflow. However, how much each water mass contributes to the water entering these basins varies seasonally. The penetration of the intermediate water (figures S1b and c) follows the seasonal cycle of flow (figure S1a). Deep inflow follows this seasonal cycle less strongly (figures S1b and c) due to the relatively consistent inflow of deep water (figure 7).

The flow rate of surface inflow has an inverse correlation to the seasonal cycle of flow due to the timing of the transient regime. Surface inflow only reaches the inner basins when the transient regime is persistent enough for the Columbia River plume to reach PRT ($\sim$2 days, figure 3) and travel the length of JdF ($\sim$8 days (Pawlowicz et al., 2019)), which only occurs during downwelling.

Summer flux in JdF closely matches estuarine flow dynamics (figure 5). This regime was expected to dominate ∼90% of the time in the summer (Thomson et al., 2007), but defining the transient regime as any period with sustained (day or longer) Columbia River inflow or with surface inflow on the southern side of the channel, it was found that no day in summer 2017 deviated from estuarine flow. The lack importance of the transient regime in summer 2017 and the similarity in summer conditions between years suggests that the complex dynamics of the transient regime may be neglected in future summer analysis.

Winter flux in JdF shows evidence of both the estuarine and transient regime (figure 5); a high velocity inflow core aligns with the typical estuarine shape, while inflow at the surface and scattered throughout the cross section highlights how the variability in flow regimes in the winter moves the dominant PRT inflow location around intermittently. The transient regime occurred about half of the time, 58% of days in winter 2016/17 and 44% in winter 2017/18, compared to the 45% expected from observations (Thomson et al., 2007). The difference between the transient regime dominance estimation in this study and those in previous estimations, can be attributed to the significant variability in interannual winter conditions overall.

4.1.3 Loop Flow

A significant portion of the water seeded at PRT in SalishSeaCast and CIOPS simulations becomes loop flow returning to cross PRT. Looped parcels in SalishSeaCast runs are parcels entrained into the upper layer and advected back out to sea (Ebbesmyer et al., 1988; MacCready et al., 2021) or pushed out of JdF due to shifts in wind direction and the associated switch between the estuarine and transient flow regimes (Thomson et al., 2007), the former largely impacting intermediate and deep water and the later primarily impacting surface water.

In CIOPS runs the looped water parcels (strait outflow) contribute similar amounts to PRT inflow as the north and offshore sources in the summer (about a quarter of total inflow), and about half of PRT inflow in the two analysed winters. In the summer this strait outflow may be due to parcels getting caught in the JdF-Eddy and advected back towards the Strait (Sahu et al., 2022), in the winter it may be outflow that is pushed back into JdF due to variable wind conditions particularly during downwelling (Giddings

& MacCready, 2017), in both seasons it could simply be water parcels entrained into the lower layer via reflux circulation (MacCready et al., 2021), or, most likely, a combination. Strait outflow returns to PRT in locations distinct from the other water masses and with minimal change in properties over its path, indicating that strait outflow undergoes little mixing, likely due to its low density.

4.2 Limitations

4.2.1 Model

Models of the real world and the studies that stem from them are inherently subject to limitations. In CIOPS analysis surface inflow in the winter was spread over the entire width of JdF, instead of focused on the southern side of the channel as expected from observations and seen in SalishSeaCast winter results; potentially due to the lower resolution of CIOPS. To account for this, “surface” inflow was defined according to parcel salinity (a close match between the models), not according to PRT inflow location, such that this inflow location disagreement did not have an impact on the surface inflow quantification.

The relatively low resolution of CIOPS may also lead to other limitations. The JdF-Canyon is a single cell wide and has a bottom cell height of 87 m, too low to accurately represent upwelled flux in a submarine canyon (Dawe & Allen, 2010), likely resolving only $\sim 80\%$ of the onshore transport through the canyon (Sahu et al., 2022); parcels flowing up the JdF-Canyon majoritively did so above 200 m when the canyon began to widen (figure S3). The location of the CUC in CIOPS, about 3.4 km offshore of where it’s present in observations (Sahu, 2019), potentially also contributed to an underestimation.

Converting the CIOPS output from daily to hourly (Beutel, 2023a) undoubtedly improved the CIOPS simulation results by adding tidal pumping, but is not completely accurate. It was assumed that baroclinic flow (which CIOPS provides as a day average) was constant over a full day; however, baroclinic variability plays a large role in tidal variability in the region. Tidal pumping is important to flow within the Salish Sea but is less important in less constricted areas (Becherer et al., 2016; MacCready et al., 2021). Previous work has shown that, despite being smaller than the tidal signal, the seasonal cycle of non-tidal currents along the British Columbia shelf is more important for the changing properties of water (Denman et al., 1982; H.J. Freeland & Thomson, 1984). Tidal pumping and mixing is also weaker in the CIOPS domain applied in this study, so while assuming that baroclinic flow has negligible diel variation surely impacted the accuracy of the tidal calculations, the impact is not expected to be severe.

4.2.2 Lagrangian Tracking

The average flow in this study at the PRT (CIOPS) and into the inner basins (SalishSeaCast) compare well to previous Eulerian estimates that do not include net tidal impacts but do include reflux circulation (Khangaonkar et al., 2017). The estimate is lower than those in studies that include both tidal impacts and reflux circulation (MacCready et al., 2021; Pawlowicz, 2001), by about one third; however, when tidal pumping is not removed from the Lagrangian estimates in this study, those at PRT are comparable to the Eulerian estimates. The addition or removal of tidally pumped parcels does not impact the flux through the inner basins.

Lower average flow estimates at the inner basins may be largely due to the fact that the Lagrangian analysis in this study solely tracked the flow of water parcels originating at PRT in order to discuss the contribution of Pacific water to the inner basins, the contribution of reflux circulation and local tidal pumping is not included while they are important contributors in the previous estimates (MacCready et al., 2021).

5 Conclusions

The inflow properties, flow magnitude, and water mass dynamics found between seasons and years in this analysis highlight the striking difference between summer and winter conditions.

In the summer, water masses from the north and offshore accounted for over 70% of the Pacific water entering the Salish Sea via JdF, unexpectedly highlighting the importance of offshore water.

In the winter, water masses from the southern boundary dominate Pacific inflow. Combined, the southern shelf water (∼60% overall) and the Columbia River plume (∼20% overall) make up over 80% of the Pacific inflow on any given day in the winter, but are poorly correlated.

The return of strait outflow to JdF is an important source of Salish Sea inflow, accounting for over a quarter of the total inflow in the summer, and around half in the winter, consistent with previous findings of significant reflux flow in JdF (Ebbesmyer et al., 1988; MacCready et al., 2021). This water mass is much less dense than the other sources and undergoes very little mixing with the other sources while on the shelf.

Lagrangian analysis of SalishSeaCast, over the same period as CIOPS analysis, quantified the success of the Pacific water masses in reaching the inner basins (Haro Region and Puget Sound), as opposed to being advected back out of JdF. Water entering in the intermediate layer (<150 m and >32 $\mathrm{g\,kg^{-1}}$ in this study, primarily north shelf and offshore water in the summer and southern shelf water in the winter) is the largest contributor to inner basin inflow year round and contributes more water to the inner basins during strong estuarine flow seen in the summer. Deep water (>150 m) flows relatively steadily into the Salish Sea, and is similarly successful to intermediate inflow. Surface water (<150 m and <32 $\mathrm{g\,kg^{-1}}$, both Columbia River water and brackish JdF outflow) reaches the inner basins mostly during winter transient conditions.

Despite being from different origins in the summer, JdF inflow has remarkably consistent properties and property variability between years is minimal. Winter conditions align with known offshore conditions (downwelling), with relatively warm and fresh inflow. However, the different water masses entering JdF have very different properties and, exhibit different properties throughout the season and between years. These factors, combined with the variability in winter water mass contributions, lead to a much larger range and significantly more variability in the inflow properties in the winter months.

While summer conditions get more attention due to the high productivity during this period, this research reveals that winter source dynamics (figures 4 and S1) are the larger driver of interannual variability. This study extended the knowledge of water mass contributions and variability to the Salish Sea, an important piece to understanding Salish Sea productivity fluctuations and its sensitivity to changing offshore conditions.

Open Research Section

Simulation setup and results files are archived at the the Federated Research Data Repository, `https://doi.org/10.20383/103.0765` (Beutel, 2023c). Analysis, and figures code are available at the following repository: `https://github.com/rbeutel/PI_SOURCE_PAPER` (Beutel, 2023b).

Acknowledgments

The authors are thankful for the opportunity to conduct research on the coast of and about the Salish Sea, the traditional, ancestral, and unceded territory of the Coast Salish peoples. We recognize their enduring presence on these waters and express our gratitude for their stewardship of this territory. We would like to thank Rich Pawlowicz, Charles Perin, and Debby Ianson for their insightful reviews of the thesis that inspired this paper, and two anonymous reviewers of this paper, all of which improved this work immensely; Doug Latornell for his work on SalishSeaCast and his computation lessons; and Michael Dunphy for sharing CIOPS-W output. This work was funded by the NSERC - CGS M scholarship to BB and NSERC - Discovery RGPIN-2022-03112 to SEA.

References

Beamish, R. J., Sweeting, R. M., & Neville, C. M. (2004). Improvement of juvenile Pacific salmon production in a regional ecosystem after the 1998 climatic regime shift. *Transactions of the American Fisheries Society*, *133*(5), 1163-1175. doi: 10.1577/T03-170.1

Becherer, J., Flöser, G., Umlauf, L., & Burchard, H. (2016). Estuarine circulation versus tidal pumping: Sediment transport in a well-mixed tidal inlet. *Journal of Geophysical Research: Oceans*, *121*(8), 6251-6270. doi: 10.1002/2016JC011640

Belluz, J. D. B., Peña, A. M., Jackson, J. M., & Nemcek, N. (2021). Phytoplankton composition and environmental drivers in the Northern Strait of Georgia (Salish Sea), British Columbia, Canada. *Estuaries and Coasts*, *22*, 1419-1439. doi: 10.1007/s12237-020-00858-2

Bennett, A. (2006). *Lagrangian fluid dynamics.* The Edinburgh Building, Cambridge, CB2 8RU, UK: Cambridge University Press.

Beutel, B. (2023a). Pacific sources of biologically significant constituents in the Salish Sea using Lagrangian particle tracking. *University of British Columbia, Electronic Theses and Dissertations (ETDs) 2008+*. doi: https://dx.doi.org/10.14288/1.0428075

Beutel, B. (2023b). *"Seasonal and interannual Salish Sea inflow origins using La-*

grangian tracking" public repository [ComputationalNotebooks]. `https://github.com/rbeutel/PI_SOURCE_PAPER`.

Beutel, B. (2023c). *Simulation output for Beutel Allen, 2023 - Pacific inflow into the Salish Sea [SimulationOutput].* doi: https://doi.org/10.20383/103.0765

Blanke, B., & Raynaud, S. (1997). Kinematics of the Pacific Equatorial Undercurrent: an Eulerian and Lagrangian approach from GCM results. [Software]. *Journal of Physical Oceanography*, *27*(6), 1038 - 1053. doi: 10.1175/1520-0485(1997)027⟨1038:KOTPEU⟩2.0.CO;2

Bograd, S. J., Schroeder, I. D., & Jacox, M. G. (2019). A water mass history of the Southern California current system. *Geophysical Research Letters*, *46*(12), 6690-6698. doi: doi.org/10.1029/2019GL082685

Brasseale, E., Grason, E., McDonald, P., Adams, J., & Maccready, P. (2019, 06). Larval transport modeling support for identifying population sources of European green crab in the Salish Sea. *Estuaries and Coasts*, *42*. doi: 10.1007/s12237-019-00586-2

Brasseale, E., & MacCready, P. (2021). The shelf sources of estuarine inflow. *Journal of Physical Oceanography*, *51*(7), 2407 - 2421. doi: 10.1175/JPO-D-20-0080.1

Brasseale, E., & MacCready, P. (2023). Seasonal wind stress direction influences source and properties of inflow to the Salish Sea and Columbia River estuary. Retrieved from `http://dx.doi.org/10.22541/essoar.169603588.89583852/v1` doi: 10.22541/essoar.169603588.89583852/v1

Chenillat, F., Rivière, P., Capet, X., Di Lorenzo, E., & Blanke, B. (2012). North Pacific Gyre Oscillation modulates seasonal timing and ecosystem functioning in the California Current upwelling system. *Geophysical Research Letters*, *39*(1). doi: https://doi.org/10.1029/2011GL049966

Davis, R. E. (1994). Lagrangian and eulerian measurements of ocean transport processes. In P. Malanotte-Rizzoli & A. R. Robinson (Eds.), *Ocean processes in climate dynamics: Global and Mediterranean examples* (pp. 29–60). Dordrecht: Springer Netherlands. doi: 10.1007/978-94-011-0870-6_2

Dawe, J. T., & Allen, S. E. (2010). Solution convergence of flow over steep topography in a numerical model of canyon upwelling. *Journal of Geophysical Research: Oceans*, *115*(C5). doi: https://doi.org/10.1029/2009JC005597

Denman, K., Freeland, H., & Mackas, D. (1982). An upwelling gyre off the west coast of Vancouver Island. *Lighthouse*, *26*, 7–9.

Ebbesmyer, C., Word, J., & Barnes, C. (1988). Hydrodynamics of estuaries. In (p. 17-49). CRC Press.

Fassbender, A. J., Alin, S., Feely, R. A., Sutton, A. J., Newton, J. A., Krembs, C., ... Pelletier, G. (2018). Seasonal carbonate chemistry variability in marine surface waters of the US Pacific Northwest. *Earth System Science Data*, *10*, 1367-1401. doi: 10.5194/essd-10-1367-2018

Foreman, M., Callendar, W., MacFadyen, A., Hickey, B. M., Thomson, R. E., & Di Lorenzo, E. (2008). Modeling the generation of the Juan de Fuca Eddy. *Journal of Geophysical Research: Oceans*, *113*(C3). doi: 10.1029/2006JC004082

Foreman, M., Crawford, W., Cherniawsky, J., Henry, R., & Tarbotton, M. (2000, 12). A high-resolution assimilating tidal model for the northeast Pacific Ocean. *Journal of Geophysical Research*, *105*, 28629-28651. doi: 10.1029/1999JC000122

Foreman, M., Pal, B., & Merryfield, W. J. (2011). Trends in upwelling and downwelling winds along the British Columbia shelf. *Journal of Geophysical Research: Oceans*, *116*(C10). doi: https://doi.org/10.1029/2011JC006995

Freeland, H., & Denman, K. (1982). A topographically controlled upwelling center of southern Vancouver Island. *Journal of Marine Research*, *40*(4), 1069-1093.

Gaydos, J. K., & Brown, N. A. (2011). Species of concern within the Salish Sea: changes from 2002 to 2011. In *Salish Sea species of concern, proceedings of the 2011 Salish Sea Ecosystem Conference, october 25-27, 2011.* Vancouver, BC.

Gaydos, J. K., & Pearson, S. F. (2011). Birds and Mammals that Depend on the Salish Sea: A Compilation. *Northwestern Naturalist*, *92*(2), 79 – 94. doi: 10.1898/10-04.1

Giddings, S. N., & MacCready, P. (2017). Reverse estuarine circulation due to local and remote wind forcing, enhanced by the presence of along-coast estuaries. *Journal of Geophysical Research: Oceans*, *122*, 10,184-10,205. doi: 10.1002/2016JC012479

Giddings, S. N., MacCready, P., Hickey, B. M., Banas, N. S., Davis, K. A., Siedlecki, S. A., ... Connolly, T. P. (2014). Hindcasts of potential harmful algal bloom transport pathways on the pacific northwest coast. *Journal of Geophysical Research: Oceans*, *119*(4), 2439-2461. doi: https://doi.org/10.1002/2013JC009622

Hailegeorgis, D., Lachkar, Z., Rieper, C., & Gruber, N. (2021). A Lagrangian study of the contribution of the Canary coastal upwelling to the nitrogen budget of the open North Atlantic. *Biogeosciences*, *18*(1), 303–325. Retrieved from `https://bg.copernicus.org/articles/18/303/2021/` doi: 10.5194/bg-18-303-2021

Haugerud, R. A. (1999). *Digital elevation model (DEM) of Cascadia, latitude 39N-53N, longitude 116W-133W. U. S. Geological Survey Open-File Report 99-369* (Tech. Rep.). U. S. Geological Survey. Retrieved from `https://pubs.usgs.gov/of/1999/0369/`

Hickey, B. (1998). Coastal oceanography of western North America from the tip of Baja California to Vancouver Island. In A. Robinson & K. Brink (Eds.), *The sea. coastal segment (18,e)* (Vol. 11, p. 345-393). John Wiley & Sons, Inc.

Hickey, B., McGabe, R., Geier, S., Dever, E., & Kachel, N. (2009, 01). Three interacting freshwater plumes in the northern California Current System. *J. Geophys. Res.*, *114*. doi: 10.1029/2008JC004907

Hickey, B., Zhang, X., & Banas, N. (2002, 10). Coupling between the California Current System and a coastal plain estuary in low river flow conditions. *Journal of Geophysical Research C: Oceans*, *107*. doi: 10.1029/1999JC000160

H.J. Freeland, W. C., & Thomson, R. (1984). Currents along the pacific coast of Canada. *Atmosphere-Ocean*, *22*(2), 151-172. doi: 10.1080/07055900.1984.9649191

Holbrook, J. R., & Halpern, D. (1982). Winter-time near-surface currents in the strait of juan de fuca. *Atmosphere-Ocean*, *20*(4), 327-339. doi: 10.1080/07055900.1982.9649149

Holdsworth, A. M., Zhai, L., Lu, Y., & Christian, J. R. (2021). Future changes in oceanography and biogeochemistry along the Canadian Pacific continental margin. *Frontiers in Marine Science*, *8*. Retrieved from `https://www.frontiersin.org/article/10.3389/fmars.2021.602991` doi: 10.3389/fmars.2021.602991

Hourston, R. A., & Thomson, R. E. (2020). *State of the physical, biological and selected fishery resources of Pacific Canadian marine ecosystems in 2020; section 8 - wind-driven upwelling/downwelling along the northwest coast of north america: timing and magnitude* (Tech. Rep.). Sidney, British Columbia: Fisheries and Oceans Canada.

Huyer, A., Barth, J., Kosro, P., Shearman, R., & Smith, R. (1998, 08). Upper-ocean water mass characteristics of the california current, summer 1993. *Deep Sea Research Part II: Topical Studies in Oceanography*, *45*, 1411-1442. doi: 10.1016/S0967-0645(98)80002-7

Ikeda, M., & Emery, W. J. (1984). A continental shelf upwelling event off Vancouver Island as revealed by satellite infrared imagery. *Journal of Marine Research*, *42*, 303-317. doi: 10.1357/002224084788502774

Jarnikova, T., Ianson, D., Allen, S., Shao, A., & Olson, E. (2022, 07). Anthropogenic carbon increase has caused critical shifts in aragonite saturation across a sensitive coastal system. *Global Biogeochemical Cycles*, *36*. doi: 10.1029/2021GB007024

Khangaonkar, T., Long, W., & Xu, W. (2017). Assessment of circulation and inter-basin transport in the Salish Sea including Johnstone Strait and Discovery Islands pathways. *Ocean Modelling*, *109*, 11-32. doi: https://doi.org/10.1016/j.ocemod.2016.11.004

Kuang, C., Stevens, S. W., Pawlowicz, R., Maldonado, M. T., Cullen, J. T., & Francois, R. (2022). Factors controlling the temporal variability and spatial distribution of dissolved cadmium in the coastal salish sea. *Continental Shelf Research*, *243*, 104761. doi: https://doi.org/10.1016/j.csr.2022.104761

Labrecque, M., Thomson, R., Stacey, M., & Buckley, J. (1994). Residual currents in Juan de Fuca Strait. *Atmosphere-Ocean*, *32*, 375-394. doi: 10.1080/07055900.1994.9649503

LaCasce, J. (2008). Statistics from Lagrangian observations. *Progress in Oceanography*, *77*(1), 1-29. Retrieved from `https://www.sciencedirect.com/science/article/pii/S0079661108000232` doi: https://doi.org/10.1016/j.pocean.2008.02.002

Lellouche, J.-M., Le Galloudec, O., Drévillon, M., Régnier, C., Greiner, E., Garric, G., ... De Nicola, C. (2013). Evaluation of global monitoring and forecasting systems at Mercator Océan. *Ocean Science*, *9*(1), 57–81. doi: 10.5194/os-9-57-2013

Levier, B., Tréguier, A., Madec, G., & Garnier, V. (2007). Free surface and variable volume in the NEMO code. *MERSEA IP report WP09-CNRS-STR03-1A*.

Lu, Y., Li, J., & Lei, J. (2017). Impacts of model resolution on simulation of mesoscale eddies in the Northeast Pacific Ocean. *Satellite Oceanography and Meteorology*, *2*(2).

MacCready, P., McCabe, R. M., Siedlecki, S. A., Lorenz, M., Giddings, S. N., Bos, J., . . . Garnier, S. (2021). Estuarine circulation, mixing, and residence times in the Salish Sea. *Journal of Geophysical Research: Oceans*, *126*(2). doi: 10.1029/2020JC016738

Mackas, D. L., Denman, K. L., & Bennett, A. F. (1987). Least squares multiple tracer analysis of water mass composition. *Journal of Geophysical Research: Oceans*, *92*(C3), 2907-2918. doi: https://doi.org/10.1029/JC092iC03p02907

Madec, G., & the NEMO team. (2016). *Nemo ocean engine* (Project Report). Retrieved from `https://www.nemo-ocean.eu/doc/`

Masson, D. (2006). Seasonal water mass analysis for the straits of Juan de Fuca and Georgia. *Atmosphere-Ocean*, *44*, 1-15. doi: 10.3137/ao.440101

Milbrandt, J. A., Bélair, S., Faucher, M., Vallée, M., Carrera, M. L., & Glazer, A. (2016). The pan-canadian high resolution (2.5 km) deterministic prediction system. *Weather and Forecasting*, *31*(6), 1791 - 1816. Retrieved from `https://journals.ametsoc.org/view/journals/wefo/31/6/waf-d-16-0035_1.xml` doi: 10.1175/WAF-D-16-0035.1

Morrison, J., Foreman, M. G. G., & Masson, D. (2012). A method for estimating monthly freshwater discharge affecting British Columbia coastal waters. *Atmosphere-Ocean*, *50*(1), 1-8. doi: 10.1080/07055900.2011.637667

Olson, E. M., Allen, S. E., Do, V., Dunphy, M., & Ianson, D. (2020). Assessment of nutrient supply by a tidal jet in the Northern Strait of Georgia based on a biogeochemical model. *Journal of Geophysical Research: Oceans*, *125*(8), e2019JC015766. doi: 10.1029/2019JC015766

Ott, M. W., & Garrett, C. J. R. (1998). Frictional estuarine flow in Juan de Fuca Strait, with implications for secondary circulation. *Journal of Geophysical Research*, *103*, 15657-15666.

Paris, C. B., Atema, J., Irisson, J.-O., Kingsford, M., Gerlach, G., & Guigand, C. M. (2013, 08). Reef odor: A wake up call for navigation in reef fish larvae. *PLOS ONE*, *8*(8), 1-8. doi: 10.1371/journal.pone.0072808

Pawlowicz, R. (2001). A tracer method for determining transport in two-layer systems, applied to the Strait of Georgia/Haro Strait/Juan de Fuca Strait estuarine system. *Estuarine, Coastal and Shelf Science*, *52*(4), 491-503. doi: 10.1006/ecss.2000.0748

Pawlowicz, R., Hannah, C., & Rosenberger, A. (2019). Lagrangian observations of estuarine residence times, dispersion, and trapping in the Salish Sea. *Estuarine, Coastal and Shelf Science*, *225*. doi: 10.1016/j.ecss.2019.106246

Pearsall, I., Schmidt, M., Kemp, I., & Riddell, B. (2021). *Factors limiting survival of juvenile chinook salmon, coho salmon and steelhead in the salish sea: Synthesis of findings of the salish sea marine survival project* (Tech. Rep.). Long Live the Kings; Pacific Salmon Foundation. Retrieved from `https://marinesurvival.wpengine.com/wp-content/uploads/2021PSF-SynthesisPaper-Screen.pdf`

Preikshot, D., Beamish, R. J., & Neville, C. M. (2013). A dynamic model describing ecosystem-level changes in the Strait of Georgia from 1960 to 2010. *Progress in Oceanography*, *115*, 28-40. doi: 10.1016/j.pocean.2013.05.020

Saha, S., Moorthi, S., Wu, X., Wang, J., Nadiga, S., Tripp, P., . . . Becker, E. (2014). The NCEP climate forecast system version 2. *Journal of Climate*, *27*(6), 2185 - 2208. doi: 10.1175/JCLI-D-12-00823.1

Sahu, S. (2019). *Characterizing the lowest oxygen waters on the southern continental shelf off Vancouver Island* (Doctoral dissertation, University of British Columbia). doi: http://dx.doi.org/10.14288/1.0385530

Sahu, S., Allen, S. E., Saldías, G. S., Klymak, J. M., & Zhai, L. (2022). Spatial and temporal origins of the La Perouse low oxygen pool: A combined Lagrangian statistical approach. *Journal of Geophysical Research: Oceans*, *127*(3). doi: https://doi.org/10.1029/2021JC018135

Schmidt, C., Schwarzkopf, F. U., Rühs, S., & Biastoch, A. (2021). Characteristics and robustness of agulhas leakage estimates: an inter-comparison study of lagrangian methods. *Ocean Science*, *17*(4), 1067–1080. Retrieved from `https://os.copernicus.org/articles/17/1067/2021/` doi: 10.5194/os-17-1067-2021

Soontiens, N., & Allen, S. E. (2017). Modelling sensitivities to mixing and advection in a sill-basin estuarine system. *Ocean Modelling*, *112*, 17-32. doi: https://doi.org/10.1016/j.ocemod.2017.02.008

Soontiens, N., Allen, S. E., Latornell, D., Souëf, K. L., Machuca, I., Paquin, J.-P., . . . Korabel, V. (2016). Storm surges in the Strait of Georgia simulated with a regional model. *Atmosphere-Ocean*, *54*(1), 1-21. doi: 10.1080/07055900.2015.1108899

Stevens, S. W., Pawlowicz, R., & Allen, S. E. (2021). A study of intermediate water circulation in the Strait of Georgia using tracer-based, Eulerian, and Lagrangian methods. *Journal of Physical Oceanography*, *51*(6), 1875 - 1893. doi: 10.1175/JPO-D-20-0225.1

Sutherland, K. C. . B. E. . M. L. . M. (2013). *Digital elevation models of british columbia, canada: Procedures, data sources, and analysis* (NOAA Technical Report). Retrieved from `https://data.nodc.noaa.gov/cgi-bin/iso?id=gov.noaa.ngdc.mgg.dem:4956;view=html`

Sutton, J. N., Johannessen, S. C., & Macdonald, R. W. (2013). A nitrogen budget for the Strait of Georgia, British Columbia, with emphasis on particulate nitrogen and dissolved inorganic nitrogen. *Biogeosciences*, *10*(11), 7179-7194. doi: 10.5194/bg-10-7179-2013

Thomson, R. (1981). *Oceanography of the British Columbia coast* (Vol. 56:291). Ottawa, Ontario: Canada Special Publications.

Thomson, R., Hickey, B. M., & LeBlond, P. H. (1989). The Vancouver Island coastal current: Fisheries barrier and conduit. In R. J. Beamish & G. A. McFarlane (Eds.), *Effects of ocean variability on recruitment and an evaluation of parameters used in stock assessment models* (Vol. 108, p. 265-296). Ottawa, Ontario: Dept. of Fish. and Oceans.

Thomson, R., & Krassovski, M. (2010). Poleward reach of the California Undercurrent extension. *Journal of Geophysical Research: Oceans*, *115*(C9). doi: 10.1029/2010JC006280

Thomson, R., Mihály, S., & Kulikov, E. (2007). Estuarine versus transient flow regimes in Juan de Fuca Strait. *Journal of Geophysical Research*, *112*. doi: 10.1029/2006JC003925

Van Sebille, E., Griffies, S. M., Abernathey, R., Adams, T. P., Berloff, P., Biastoch, A., ... Zika, J. D. (2018). Lagrangian ocean analysis: Fundamentals and practices. *Ocean Modelling*, *121*, 49-75. doi: https://doi.org/10.1016/j.ocemod.2017.11.008

Vecchioni, G., Cessi, P., Pinardi, N., Rousselet, L., & Trotta, F. (2023). A lagrangian estimate of the mediterranean outflow's origin. *Geophysical Research Letters*, *50*(14), e2023GL103699. doi: https://doi.org/10.1029/2023GL103699

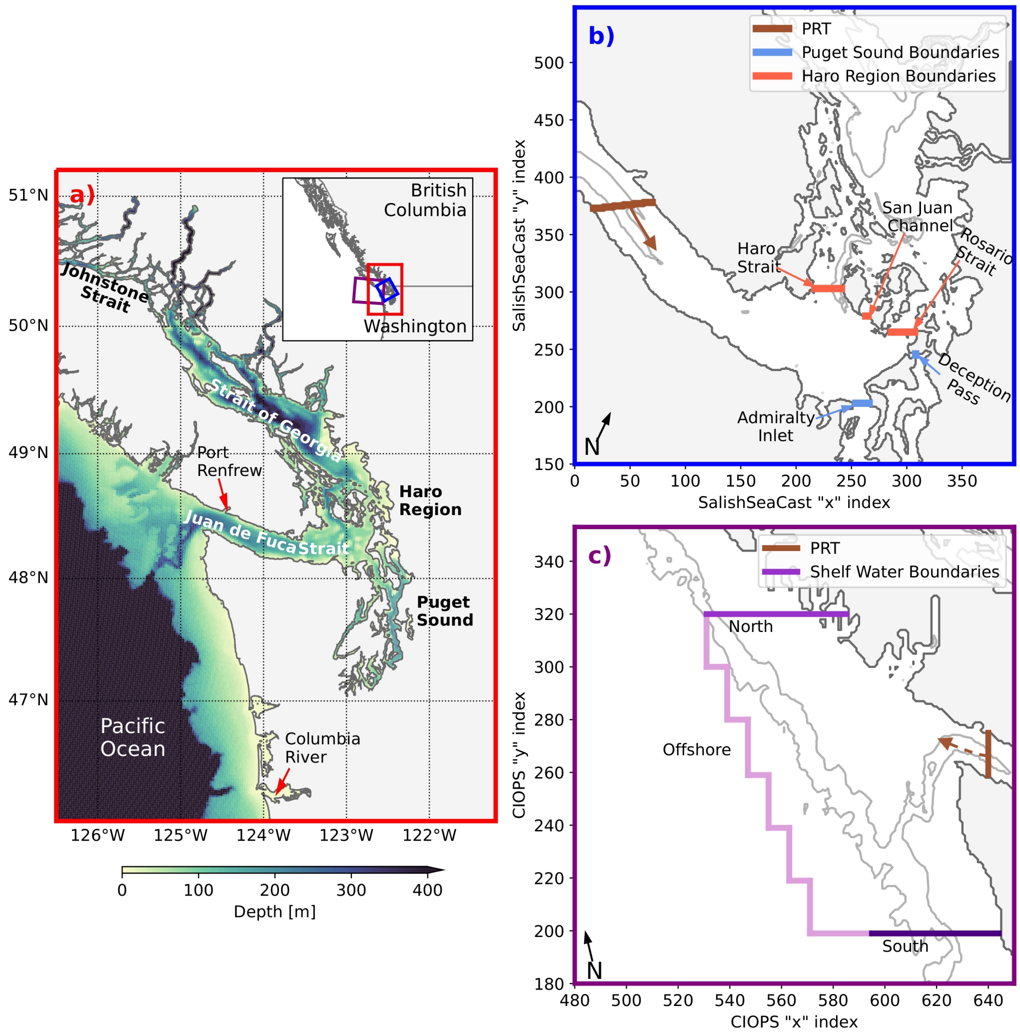

Figure 1: a) Map of the Salish Sea with bathymetry. Boundaries used for Ariane runs b) within the Salish Sea using SalishSeaCast and c) on the shelf using CIOPS with 200 m and 1000 m isobaths shown in grey (depths do not reach 1000 m in the Salish Sea so there is solely the 200 m isobath). The areas shown in the three sub-figures is show in the inset with the box colour corresponding to the figure border: a) red, b) blue, and c) purple. Note that the two models have different projections, b and c are here plotted by model index; north is noted by an arrow. The brown "PRT" boundary was used as the initialisation cross-section in both simulations. Brown arrows at the PRT boundary show the direction of integration, b) forward tracking of PRT inflow (solid line) to measure its destination, c) backwards tracking of PRT inflow (dashed line) to measure its source.

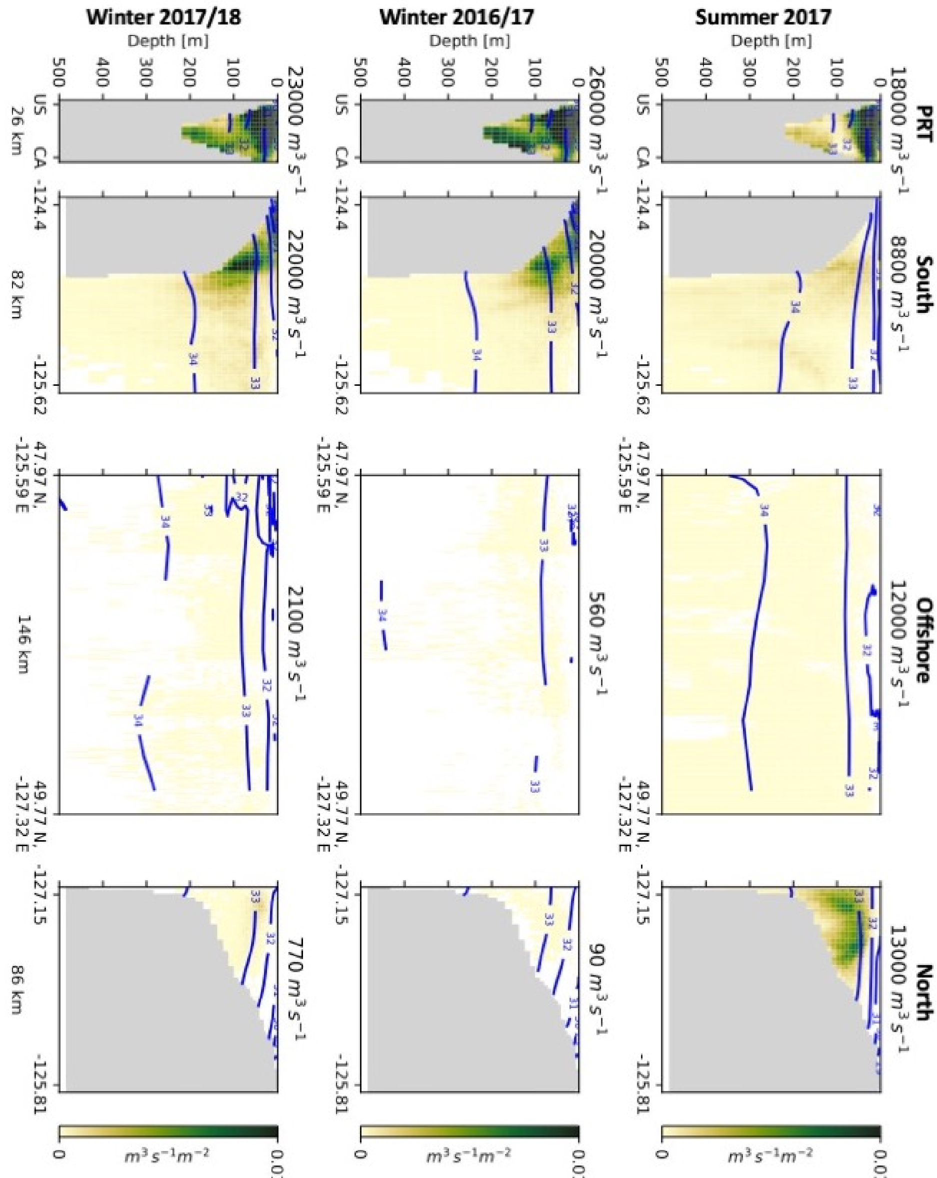

Figure 2: Source water flux density across the analysis boundaries in CIOPS Lagrangian simulations. Strait outflow (left) and Pacific water across the north (center left), south (center right), and offshore (right) cross sections in the a) Summer 2017, b) Winter 2016/17, and c) Winter 2017/18. Note that the left edge of the southern cross-section in the above figure is connected to the left side of the offshore cross-section, and the left side of the north cross-section to the right side of the offshore cross section (figure 1c). Mean seasonal salinity contours (blue) are shown in units of $\mathrm{g\,kg^{-1}}$.

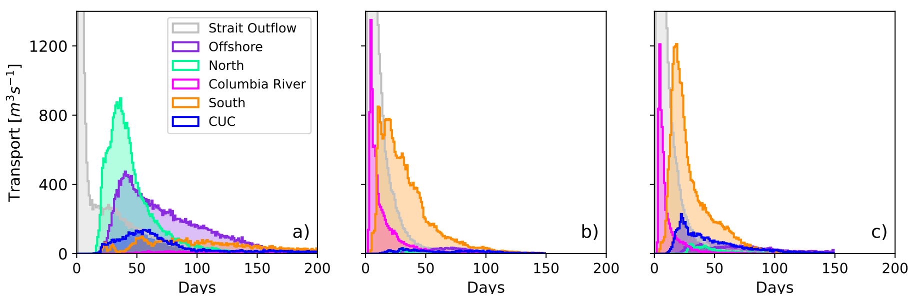

Figure 3: Simulation time (water parcel age) between the outer boundaries and PRT in CIOPS runs in a) Summer 2017, b) Winter 2016/17, and c) Winter 2017/18.

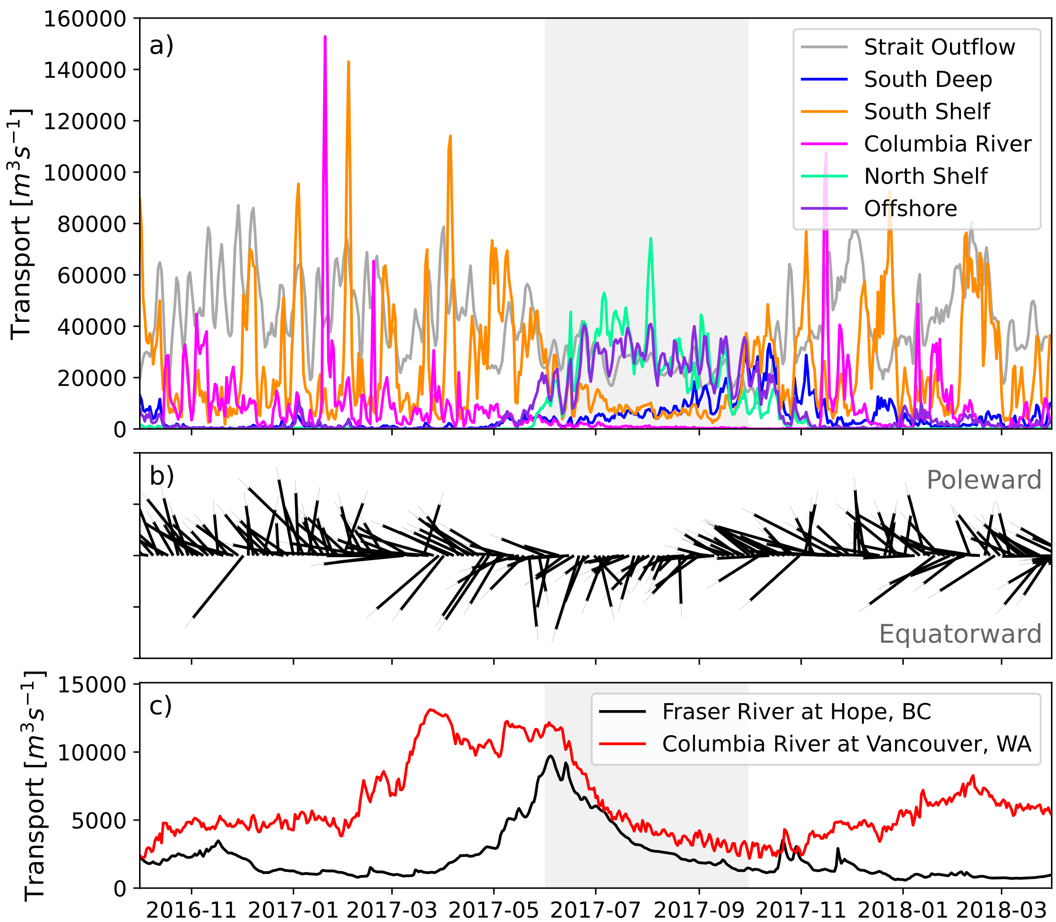

Figure 4: a) Daily inflow to PRT from Pacific sources, and a four day rolling average of the contribution of strait outflow to PRT inflow. Conditions that may impact flow to PRT: b) wind direction and relative speed along the continental shelf at La Push, Washington (70 km south of JdF), and c) river flow from the Fraser River at Hope, British Columbia and Columbia River at Vancouver, Washington. Summer 2017 (upwelling) is highlighted in grey.

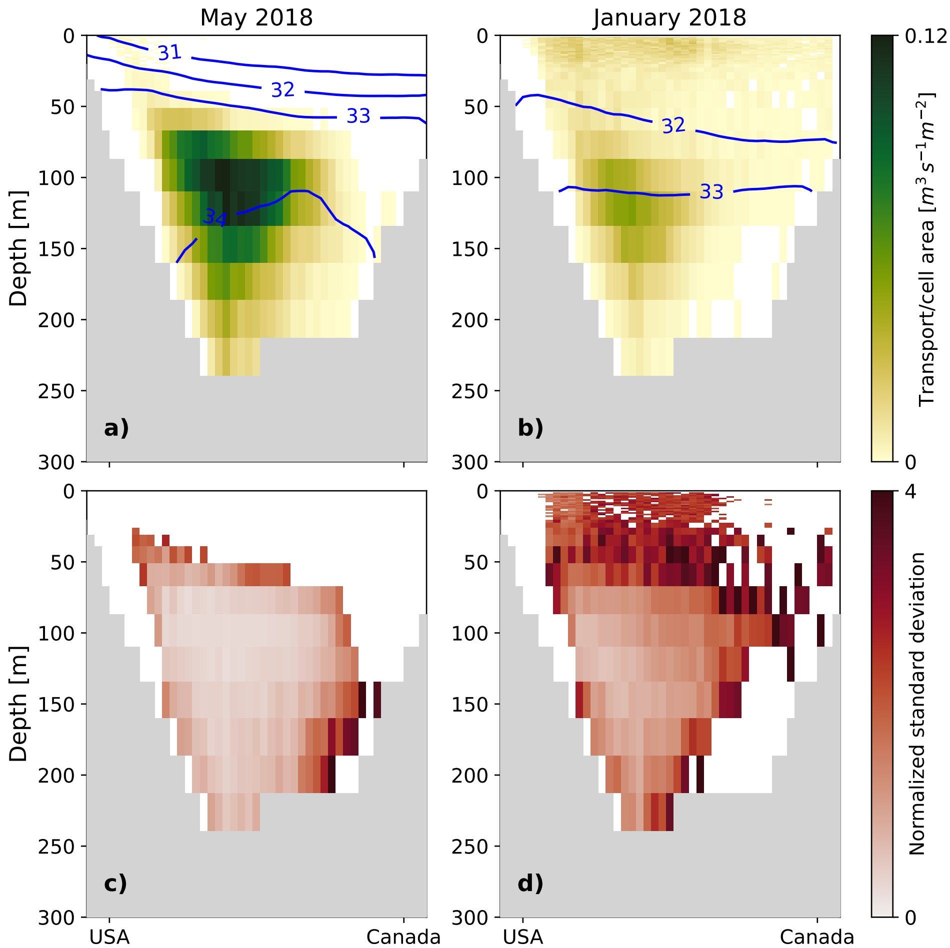

Figure 5: Flux of water parcels crossing PRT that reach the inner boundaries in a) May 2018 (left), a typical entirely estuarine summer month, and b) January 2018, a winter month with marked shifts between flow regimes. Mean monthly salinity contours (blue) are shown in units of $\mathrm{g\,kg^{-1}}$. The standard deviation in flow normalised by the average flow through each cell in c) May 2018 and d) January 2018, showing variability in flow structure during these respective periods. Cells with flow rates less than $0.006\,\mathrm{m^3m^{-2}s^{-1}}$ were removed from the standard deviation calculation.

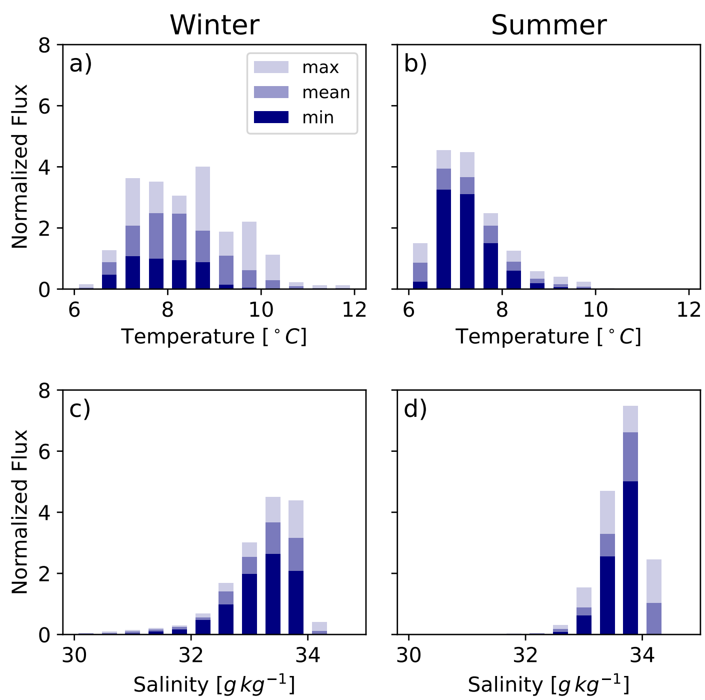

Figure 6: Histograms of transport weighted a,b) temperature and d,c) salinity of water parcels at PRT that reach the Haro Region or Puget Sound in the a,c) winter and b,d) summer months (Hourston & Thomson, 2020) over the five year simulation. Note the large interannual variability (difference between minimum and maximum) in the winter temperatures compared to the summer. Transports are normalized by the average seasonal transport.

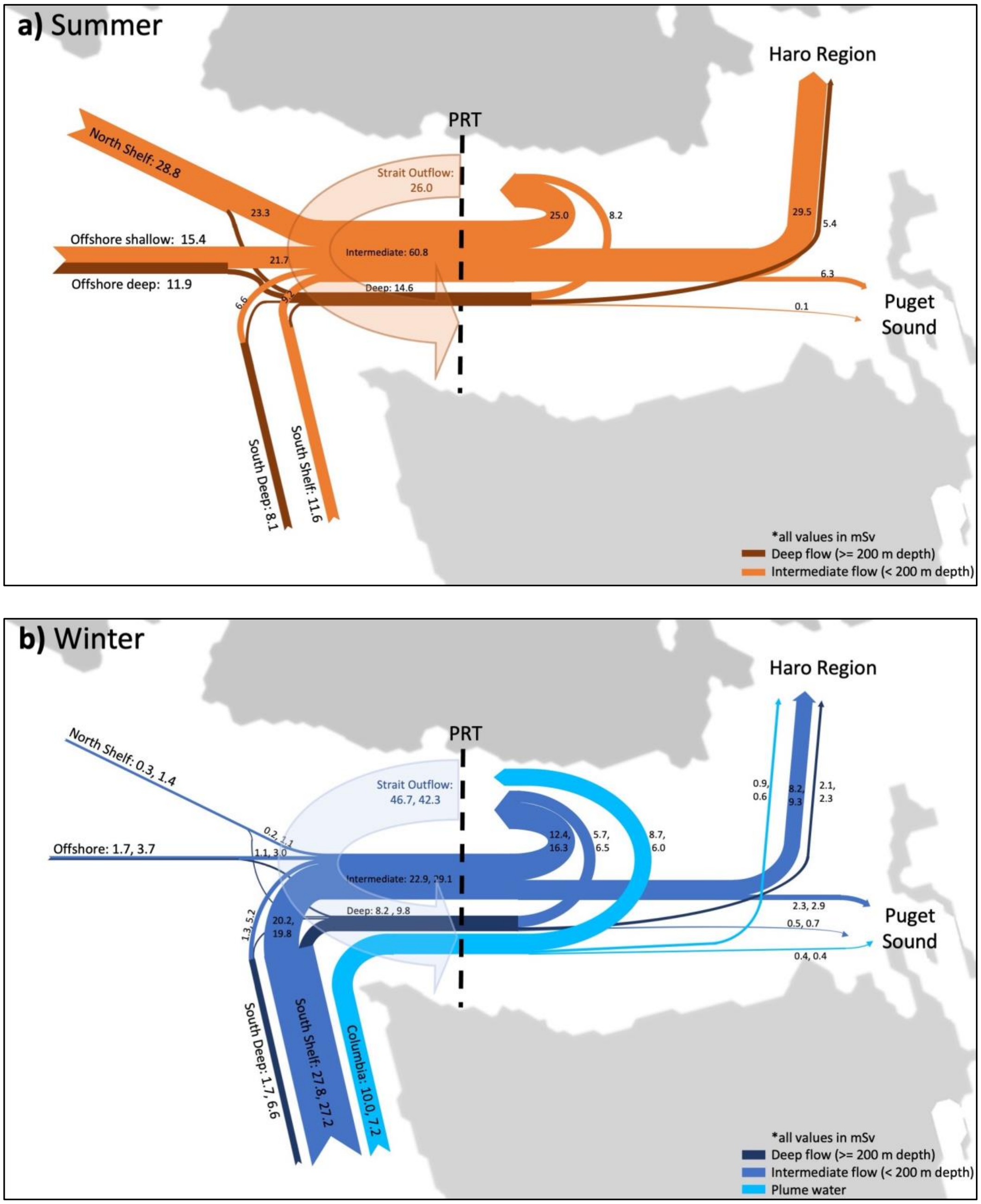

Figure 7: Water mass contributions in the a) summer 2017 and b) winters 2016/17 and 2017/18. All values are displayed in mSv ($10^3\,\mathrm{m^3 s^{-1}}$), based upon the shelf transports in CIOPS analysis and PRT to inner basin percentage contributions in table 2. Winter flows for 2016/17 and 2017/18 are both shown, in that order. Line thickness is an approximation of magnitude but is not to scale.